Electroexcitation of giant multipole resonances in ^{208}Pb

Mamiko Sasao* and Y. Torizuka
Laboratory of Nuclear Science, Tohoku University, Tomizawa, Sendai, Japan
(Received 23 October 1975; revised manuscript received 7 September 1976)

Electroexcitation of the nuclear continuum for ^{208}Pb at excitation energies up to 100 MeV has been measured at momentum transfers in the range from 0.45 to 1.2 fm^{-1}. Unfolding of the radiation tail was performed using a tail function which takes into account the multiple-photon emission effect. The spectra at these momentum transfers deviate significantly from the prediction of the Fermi-gas model but are consistent with the sum of the multipole strengths of the random-phase approximation; the excess cross section on the low excitation energy side indicates the excitation of multipole resonances. A series of ^{208}Pb spectra at low momentum transfers was expanded into $E1$, $E2$ ($E0$), $E3$, and higher multipole components using the q dependence of the Tassie model for isoscalar modes and the Goldhaber-Teller or Steinwedel-Jensen model for isovector modes. The giant dipole resonance thus obtained is consistent with that from photoreactions. Isoscalar and isovector giant quadrupole resonances are seen, respectively, at 11 and 22.5 MeV and an octupole resonance at 16 MeV. A monopole resonance is suggested at 13.5 MeV. The reduced $|\langle r^2\rangle|^2$, $B(E1)$, $B(E2)$, and $B(E3)$ consume most of the corresponding energy weighted sum rule if the q dependences of the Tassie and Goldhaber-Teller models are assumed. The results with these models are consistent with the random-phase approximation.

[NUCLEAR REACTION ^{208}Pb(e,e'), measured $(E_{e'}, \theta_{e'})$, E_x=7.4–100 MeV, q=0.45–1.2 fm^{-1}, reduced $|\langle r^2\rangle|^2$, $B(E1)$, $B(E2)$, $B(E3)$ for giant multipole resonances, multipole expansion analysis.]

I. INTRODUCTION

Since new giant resonances have been discovered through inelastic electron scattering[1-3] and hadron scattering,[4] much interest in both experiment and theory has been focused on this topic.[5] The giant multipole resonances (GMR) have generally been observed as bumps riding on the smooth nuclear continuum. In order to deduce the GMR, the continuum was empirically divided into resonance and background parts. Hence, a large uncertainty in the GMR excitation arises from the approximation used for the background. Usually, the background consists of experimental background, radiation tails, and, possibly, parts of other resonance states or quasielastic scattering.[6,7] Here we wish to propose a new method of extracting the GMR.

Difficulties arise from the large radiation tails due to the degradation of electron energies through radiation and collision losses. The contributions must be subtracted correctly from the measured spectra. We use here a tail function which takes into account the multiple-photon emission effect.[8] Next, the unfolded spectrum should be separated into longitudinal and transverse parts because the continuum contains contributions from the transverse form factor even at forward angles.[7] Then, if the q dependence of the multipole states are known, a set of several longitudinal or transverse spectra may be decomposed into multipole states without any assumption about the background. For this purpose, the spectra are divided into successive bins of equal intervals and are expanded, channel by channel, into the different multipoles. This approach can predict the position and strength of any multipole resonances.[9]

The present analysis, however, depends on the nuclear model employed.[10,11] For the isovector excitations, we have used quite different models, i.e., the Goldhaber-Teller model in which the oscillation occurs at the nuclear surface, and the Steinwedel-Jensen model in which the charge oscillation is distributed throughout the volume of the nucleus. We will discuss these choices of the nuclear model.

A series of ^{208}Pb spectra has been expanded into $E1$, $E2$, and $E3$, and higher multipole components. In electron scattering the $E0$ form factor cannot be distinguished from the $E2$ form factor. The monopole resonance may be partly contained in the $E2$ strength distribution.

Many GMR data from inelastic hadron scattering have recently been accumulated.[5,12] Studies of the GMR with various kinds of projectiles are complementary. For example, electrons can excite strongly both $E0$ and $E2$, whereas hadrons excite $E2$ strongly but $E0$ only weakly except at specific angles. Possible evidence for the 0^+ state in ^{208}Pb will be presented by comparing the excitations seen with various projectiles.

II. FORM FACTORS, TRANSITION DENSITIES, AND MODELS

In the plane wave Born approximation (PWBA) the differential cross section for inelastic electron scattering is given by[13,14]

$$d^2\sigma/d\Omega dE_2 = \sigma_{\text{Mott}} |W(q,\omega)|^2, \tag{1}$$

$$\sigma_{\text{Mott}} = (Z\alpha)^2 \cos^2\tfrac{1}{2}\theta / 4E_1^2 \sin^4\tfrac{1}{2}\theta, \tag{2}$$

where $|W|^2$ is the total differential form factor (or relative cross section) defined by this relation, E_1 and E_2 are the initial and final electron energies, and ω is the excitation energy. $|W|^2$ is further expressed in PWBA as

$$|W(q,\omega)|^2 = \left(\frac{\Delta^2}{q^2}\right)^2 |W_L(q,\omega)|^2 + \left(\tfrac{1}{2}\frac{\Delta^2}{q^2} + \tan^2\tfrac{1}{2}\theta\right) |W_T(q,\omega)|^2, \tag{3}$$

where $|W_L|^2$ is the Coulomb or longitudinal form factor, $|W_T|^2$ is the transverse form factor, and q and Δ are the three- and four-momentum transfer, respectively. This relation may be used to separate the $|W_L|^2$ and $|W_T|^2$ (a Rosenbluth plot). The form factor $|F(q)|^2$ is related to $|W|^2$ by

$$|F_{\substack{T\\L}}(q)|^2 = \int_\omega |W_{\substack{T\\L}}(q,\omega)|^2 d\omega. \tag{4}$$

For medium and heavy nuclei, however, the cross section is not described correctly by the PWBA. The effect of the Coulomb distortion can be partly taken into account if we use an effective momentum transfer[15]

$$q_{\text{eff}} = q(1 + \tfrac{3}{2}Z\alpha/E_1 R), \tag{5}$$

where R is the uniform nucleus radius. For the usual calculation of the inelastic electron scattering cross section, we use the distorted wave Born approximation (DWBA).[16]

The form factors of $J_i = 0$ nuclei can be written within the PWBA as

$$|F(q)|^2 = \frac{4\pi}{Z^2} \left| \int \rho^L_{tr}(r) j_L(qr) r^2 dr \right|^2, \tag{6}$$

where ρ^L_{tr} is defined as

$$\rho^L_{\text{tr}} = \langle J_f \| \hat{\rho}_L \| J_i \rangle. \tag{7}$$

The reduced transition probabilities can be written as

$$B(EL) = \left| \int \rho^L_{\text{tr}}(r) r^{L+2} dr \right|^2. \tag{8}$$

The $\langle r^2 \rangle$ matrix element for the monopole transition may be obtained from

$$|\langle r^2 \rangle|^2 = 4\pi \left| \int \rho^{L=0}_{\text{tr}}(r) r^4 dr \right|^2. \tag{9}$$

For the isoscalar ($T=0$) collective states the transition densities are given by

$$\rho^L_{\text{tr}}(r) = N r^{L-1} d\rho/dr \quad L \neq 0 \text{ (Tassie model)},[17] \tag{10}$$

$$= N \frac{1}{r^2} \frac{d}{dr}(r^3 \rho) \quad L = 0 \text{ (breathing mode)},[18] \tag{11}$$

where ρ is the ground state charge distribution and N is the normalizing factor. Noble,[19] Fallieros,[20] and Ui and Tsukamoto[21] have studied the sum rules for form factors and have shown that when the strength is concentrated in one specific state the transition density of the corresponding state is given by the same form as that of the Tassie model. A transition density resembling that of the Tassie model[17,18] is also obtained from the random phase approximation (RPA).[11]

For the isovector ($T=1$) giant dipole resonance (GDR), the Goldhaber and Teller (GT) model is well known.[22] In this model, the transition densities are given by

$$\rho^{\text{GT}}_{\text{tr}}(r) = C r^{L-1} d\rho/dr. \tag{12}$$

This shape is precisely the same as that of the Tassie model, and is also derived from the energy-weighted sum rule (EWSR)[20,21] if the exchange terms in the Hamiltonian are neglected. Another model for the isovector GMR is given by Steinwedel, Jensen, and Jensen (SJ),[23] in which

$$\rho^{\text{SJ}}_{\text{tr}}(r) = C' j_L(k_L r), \quad r < R, \tag{13}$$

where R is the nucleus uniform radius, with k_L determined from

$$\frac{d}{dr} j_L(k_L R) = 0.$$

The transition density we used here was normalized so that $B(EL)$ or $|\langle r^2 \rangle|^2$ is equal to 1 in units of MeV^{-2L} or MeV^{-4}, respectively. We have used here the ground-state charge density for ^{208}Pb obtained at Mainz[24] for the Tassie-model calculations and that obtained at Stanford[25] for the calculation of other models. The effect of the difference of these charge distributions is included in the 6% uncertainty of the DWBA calculation in the region of interest. As shown in Fig. 1, the isoscalar $E0$ form factor cannot be distinguished from the isoscalar $E2$ form factor. The difference between the SJ- and GT-model form factors is large. The transition densities for the SJ and GT models for the dipole state are shown in Fig. 2, where the SJ-model transition density modified to the shape[26] $\rho_{\text{tr}} \propto r\rho$ is also shown. The remarkable difference between the SJ and GT models is evident in Fig. 2. The SJ-model transition density is large well

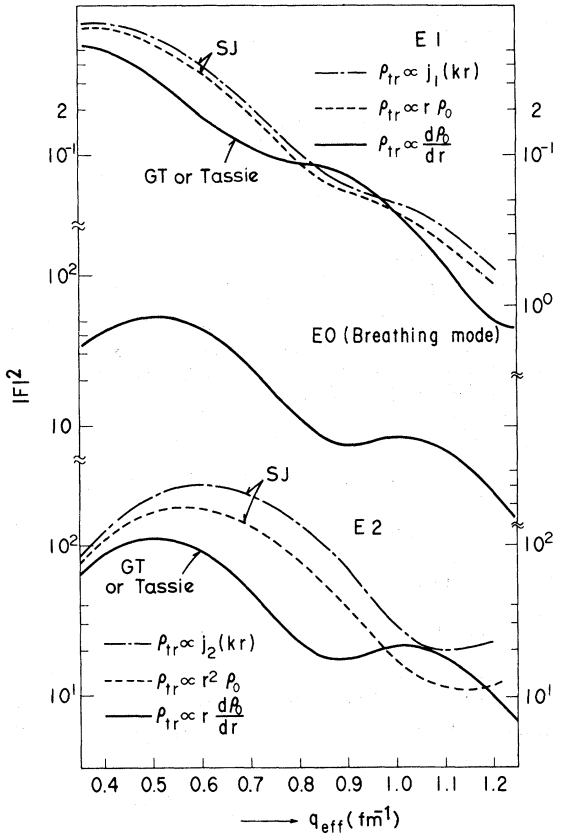

FIG. 1. Form factors calculated with the DWBA code where ρ_{tr} is normalized so that $B(EL)$ or $|\langle r^2\rangle|^2$ (for $E0$ transition) should be 1 in the unit of MeV^{-2L} or MeV^{-4}, respectively.

inside the nucleus, in contrast to the GT model in which ρ_{tr} peaks at the nuclear surface.

III. EXPERIMENT

The experiment has been performed using beams of the Tohoku 300-MeV electron linear accelerator. The beams were monitored by a secondary-emission monitor (SEM). The efficiency of the SEM was calibrated against a Faraday cup. The electrons scattered from the target were analyzed by a double-focusing magnetic spectrometer ($\theta = 169.7°$) of 100-cm central radius of curvature. The electrons were detected by a 33-channel detector system, which covers a 3.3% range in momentum. Each channel consisted of three Li-drifted silicon detectors working as a counter telescope. Experimental details may be found elsewhere.[27]

Energy spectra of inelastically scattered electrons were measured at momentum transfers ranging from 0.447 to 1.560 fm^{-1}. A 99.5% enriched ^{208}Pb target was employed. Beam intensities were changed from 10^{-9} to 5×10^{-7} amperes so that counting rates were within the limit of 5% dead-time correction. Current monitor response and detector efficiencies were determined experimentally to be constant within 1% for the entire range of intensities and electron energies used in the experiment. The incident electron energies, scattering angles, target thickness, maximum excitation energy measured, and effective momentum transfer q_{eff} at 13.5 MeV are tabulated in Table I. The measured elastic cross sections are normalized to the cross section calculated by using the ground-state charge distribution obtained at Mainz.[24] The data were taken with an overall energy resolution of 0.15%.

The so-called instrumental scattering (target-in background) may be explained as electrons scattered from the vacuum chamber wall.[28] We have investigated this effect by shifting the spectrometer magnetic field above that corresponding to the elastic scattering peak. In this case electrons scattered from the target probably hit the inner wall of the spectrometer vacuum chamber. No

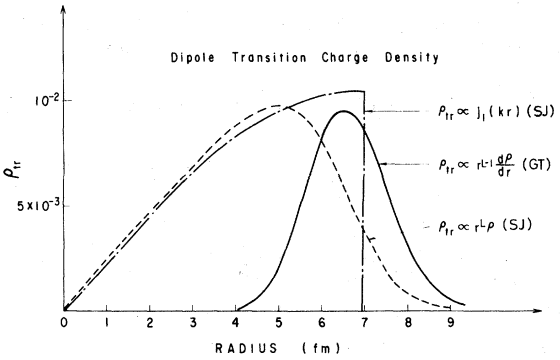

FIG. 2. Transition densities corresponding to the giant dipole resonance normalized to be $\int\rho_{tr}r^2dr=1$.

TABLE I. The experimental conditions of the measured spectrum and effective momentum transfers.

E_0 (MeV)	θ (deg)	Target thickness ($\mathrm{mg/cm^2}$)	Maximum excitation energy measured (MeV)	q_{eff} at 13.5 MeV
183	35	50	31	0.617
215	35	100	37	0.714
250	35	100	36	0.821
150	30	50	26	0.447
250	25	50	88	0.593
250	35	50	68	0.821
250	52	50	120	1.193
250	70	50	34	1.560
124	116	50	29	1.217
106.4	155	100	36	1.223

noticeable background or bumps were observed under these conditions. This is, however, indirect demonstration for the absence of the instrumental scattering; the possibility for the appearance of this effect in the observed spectra still remains.

IV. UNFOLDING OF THE RADIATION TAIL

Incident and outgoing electrons lose energy by interacting with the internal radiation field (Schwinger correction), by bremsstrahlung loss when passing through the target, and by collision with the atomic electrons.

The observed cross section integrated over the nth bin [the interval $\Delta E^{(n)}$] can be written as follows[29]:

$$\int_{\Delta E_2^{(n)}} \left(\frac{d^2\sigma}{d\Omega dE_2}\right)_{\text{obs}} dE_2 = \left(\frac{d\sigma}{d\Omega}\right)^{(n)} K(\tfrac{1}{2}\Delta E^{(n)}) + \sum_{m=0}^{n-1} \int_{\Delta E_2^{(m)}} \left(\frac{d^2\sigma}{d\Omega dE_2}\right)_{\text{tail}} dE_2 , \tag{14}$$

where $(d\sigma/d\Omega)^{(n)}$ is the nonradiative cross section of the nth bin. The correction factor $K(\Delta E)$ is the product of the $K^S(\Delta E)$, $K^B(\Delta E)$, and $K^C(\Delta E)$ corresponding to the Schwinger, bremsstrahlung, and collision corrections, respectively.

(a) The Schwinger correction factor for both elastic and inelastic scattering can be given as[30]

$$K^S(\Delta E) = e^{-\delta_S(\Delta E)}, \tag{15}$$

$$\delta_S(\Delta E) = \frac{2\alpha}{\pi}\left(\left\{\ln\left[\frac{(E_1E_2)^{1/2}}{\Delta E}\right] - \tfrac{13}{12}\right\} \times \left[\ln\left(\frac{q^2}{m_e^2}\right) - 1\right] + \tfrac{17}{36} + \tfrac{1}{4}\ln^2\left(\frac{E_1}{E_2}\right) + \tfrac{1}{2}\left[\tfrac{1}{6}\pi^2 - L_2(\cos^2(\tfrac{1}{2}\theta))\right]\right), \tag{16}$$

where higher-order terms are included by exponentiation.

(b) The probability for an electron of kinetic energy E traversing a thickness t to emit a photon of energy between ϵ and $\epsilon + d\epsilon$ is given by[31]

$$f_{\text{rad}}(E, \epsilon, t)dE = \frac{t}{\epsilon}\left[1 - \eta\frac{E-\epsilon}{E} + \left(\frac{E-\epsilon}{E}\right)^2\right]d\epsilon , \tag{17}$$

where t is measured in units of radiation length χ_0, 6.4 g/cm^2 for lead,[32] and

$$\eta = \tfrac{2}{3} - \tfrac{1}{9}[\ln(183Z^{-1/3})]^{-1}.$$

If we assume that the energy loss comes from only one photon emission, the bremsstrahlung correction is

$$\bar{K}^B(\Delta E) = 1 - \int_{\Delta E}^{E} f_{\text{rad}}(E, \epsilon, t)d\epsilon = 1 - \delta_B , \tag{18}$$

$$\delta_B = t\left[-(\tfrac{3}{2} - \eta) + (2-\eta)\ln\frac{E}{\Delta E} + (2-\eta)\frac{\Delta E}{E} - \frac{1}{2}\left(\frac{\Delta E}{E}\right)^2\right]. \tag{19}$$

Friedrich[8] suggested the introduction of exponentiation for higher-order terms,

$$K^B(\Delta E) = e^{-\delta_B}. \tag{20}$$

With this choice, the radiation probability $P_{\text{rad}}(E, \epsilon, t)$ which considers multiple-photon emission must satisfy

$$1 - \int_{\Delta E}^{E} P_{\text{rad}}(E, \epsilon, t)d\epsilon = \int_0^{\Delta E} P_{\text{rad}}(E, \epsilon, t)d\epsilon = K^B(\Delta E). \tag{21}$$

Then we obtain

$$P_{\text{rad}}(E, \epsilon, t)d\epsilon = f_{\text{rad}}e^{-\delta_B(\epsilon)}d\epsilon = f_{\text{rad}}K^B(\epsilon)d\epsilon \tag{22}$$

instead of (17).

(c) Friedrich[8] has suggested that the following form can be used to good accuracy for the collision loss near the peak:

$$K^C(\Delta E) = \begin{cases} 0.6081 - 0.0074\lambda + 0.1646\ln\lambda - 0.1457/\lambda, & 1 < \lambda < 14, \\ 1 - 1/\lambda, & 14 < \lambda, \end{cases} \tag{23}$$

where $\lambda = \Delta E/\Delta E_0$, $\Delta E_0 = 0.154(Z/A)T$, and T = target thickness in g/cm^2. The energy loss probability due to collisions can be given by

$$P_{\text{col}}(E, \epsilon, t) = \begin{cases} \frac{1}{\Delta E_0}(-0.0074 + 0.1646/\lambda + 0.1457/\lambda^2, & 1 < \lambda < 14, \\ \frac{1}{\Delta E_0}1/\lambda^2, & 14 < \lambda. \end{cases} \tag{24}$$

(d) For the internal radiation tail we used the peaking approximation formula given by Mo and Tsai,[33]

$$\left(\frac{d^2\sigma}{d\Omega dE_2}\right)_S = f_S(E_1 - \omega, k)\frac{d\sigma}{d\Omega}(E_1, E_1 - \omega) + f_S(E_1, k)\frac{d\sigma}{d\Omega}(E_2 + \omega, E_2), \tag{25}$$

$$f_S(E, k) = \frac{\alpha}{\pi k}\left\{\ln\frac{\Delta}{m_e}\left[1 + \left(\frac{E-k}{E}\right)^2\right] - \frac{E-k}{E}\right\}, \tag{26}$$

where k is the emitted photon energy and $(d\sigma/d\Omega)(E_1, E_2)$ is the nonradiative PWBA cross section for the incident energy E_1 and scattered energy E_2. Compared with the nonpeaking cross section given

by Maximon and Isabelle,[34] the approximate form (26) can be used up to 50 MeV within an error of 3%.

Equations (25) and (26) are based on the first Born approximation with one photon emission. Higher-order terms for the interaction with the nuclear potential can be taken into account by replacing the cross section $(d\sigma/d\Omega)(E_1, E_2)$ by that of the DWBA. Higher-order terms for the interaction with the internal radiation field (multiple-photon emission) cannot be neglected. Also, the tail function must be calculated by convoluting the contributions from the internal and external bremsstrahlung and from collisions. Friedrich[8] suggested that internal and external bremsstrahlung contributions can be convoluted near the elastic peak as follows:

$$\frac{d^2\sigma}{d\Omega\, dE_2}=\left\{[f_S(E_1-\omega,k)+f_{\rm rad}(E_1-\omega,k,\tfrac{1}{2}t)+P_{\rm col}(E_1-\omega,k,\tfrac{1}{2}t)]\frac{d\sigma}{d\Omega}(E_1,E_1-\omega)\right.$$
$$\left.+[f_S(E_1,k)+f_{\rm rad}(E_1,k,\tfrac{1}{2}t)+P_{\rm col}(E_1,k,\tfrac{1}{2}t)]\frac{d\sigma}{d\Omega}(E_2+\omega,E_2)\right\}K^S(k)K^B(k), \quad (28)$$

where $k+\omega\simeq E_1-E_2$. Formulas (14) and (28) were used in the unfolding procedure for the observed cross sections. The cross sections for the elastic peak and first 3^- inelastic peak for different incident energies, $(d\sigma/d\Omega)(E_2+\omega, E_2)$, were obtained by multiplying $(d\sigma/d\Omega)(E_1, E_1-\omega)$ by the ratio of the calculated cross sections. The other inelastic cross sections were obtained by multiplying by the ratios of the Mott cross sections. The effect of the inelastic form factor in the region of interest was examined and found to be small.

The spectrum unfolded by the previously used radiation tail formula[7] was negative in the region just below the elastic peak. This failure was, to a large extent, removed by using the present formulas. The raw and unfolded spectra at 250 MeV, 25°, are shown in Fig. 3. The cross sections between the elastic peak and inelastic 3^- peak at 2.61 MeV vanished within the statistical error for all the spectra in Table I, indicating that the unfolding is satisfactory. The negative cross section seen at large energy losses (~80 MeV) is much smaller than that obtained by the previously used formula. The same unfolding was also applied to the ^{90}Zr cross sections.[36] The results are quite satisfactory.

$$[2f_S(E_1,\epsilon)+f_{\rm rad}(E_1,\epsilon,t)]K^S(\epsilon)K^B(\epsilon,t)\frac{d\sigma}{d\Omega}(E_1,E_1), \quad (27)$$

where f_S and $f_{\rm rad}$ are the respective probabilities for one-photon emission. We have approximated the multiple-photon emission effect by multiplying the one-photon emission probabilities by the correction factor $K^S(\epsilon)K^B(\epsilon)$. A similar form was proposed by Tsai.[35] Together with the collision-loss probability folded numerically, the tail function (27) provides a good fit to the experimental data for ^{208}Pb between the elastic and first 3^- peaks.

Considering that the collision term decreases rapidly as the energy loss increases, we can approximate the tail function by

V. QUASIELECTRIC ELECTRON SCATTERING

Quasielastic electron scattering appears as a large bump centered at $q^2/2M^*$ with a width of $2qk_F/M^*$ for momentum transfers $q \geq 2k_F$, where M^* is the effective nucleon mass and k_F the Fermi momentum.[13] For $q < k_F$ the cross section is re-

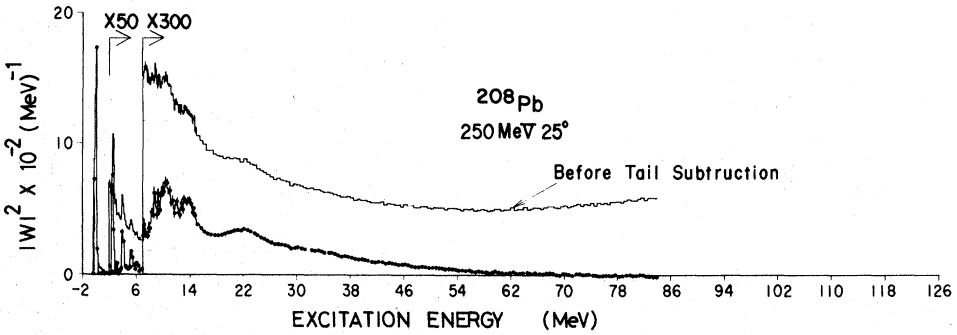

FIG. 3. Spectrum at 250 MeV, 25° before (upper) and after (lower part) the subtraction of the radiation tail.

stricted by the Pauli principle and the peak cannot be given by the simple form as a function of q. In order to investigate quasielastic scattering at low q, the present measurement was carried out in an excitation energy range up to 100 MeV.

Quasielastic electron scattering corresponding to the spectra at 250 MeV, 25°, 35°, and 52°, was calculated using the Fermi-gas model with $M^* = 0.8M$ and $k_F = 265$ MeV, consistent with currently accepted values.[37] The results are compared with the experimental spectra in Fig. 4. The measured spectra are different from the Fermi-gas model predictions, with a much larger fraction of the total strength at low excitation energies. This observation suggests that the excess cross section results from the excitation of the giant multipole resonances and involves the residual interaction which has been neglected in the simple quasielastic model.

The measured spectra are also compared with more sophisticated models which include nucleon-nucleon correlations. Random phase approximation (RPA) calculations[38-40] employing large configuration spaces and the Skyrme interaction have been performed. Reference 40 presents the spectral shapes for the isoscalar and isovector $E0$, $E1$, $E2$, $E3$, and $E4$ transition strengths up to an excitation energy of 40 MeV. The cross sections were calculated from these strength distributions using the momentum-transfer dependence of the Tassie model for the $T = 0$ states and the GT or SJ model for the $T = 1$ states. The results are shown in Fig. 4. The sum of the theoretical form factors obtained with the GT model is in excellent agreement with the experimental form factor at 250 MeV and 25°, but the theoretical form factor obtained with the SJ model is much larger than the observed one. The discrepancy between theory (using the GT model) and experiment is seen to increase with increasing momentum transfer. This effect may be removed if we include the multipole states higher than $E4$. The observed spectra at small values of q and ω may be regarded as sums of the multipole resonance states.

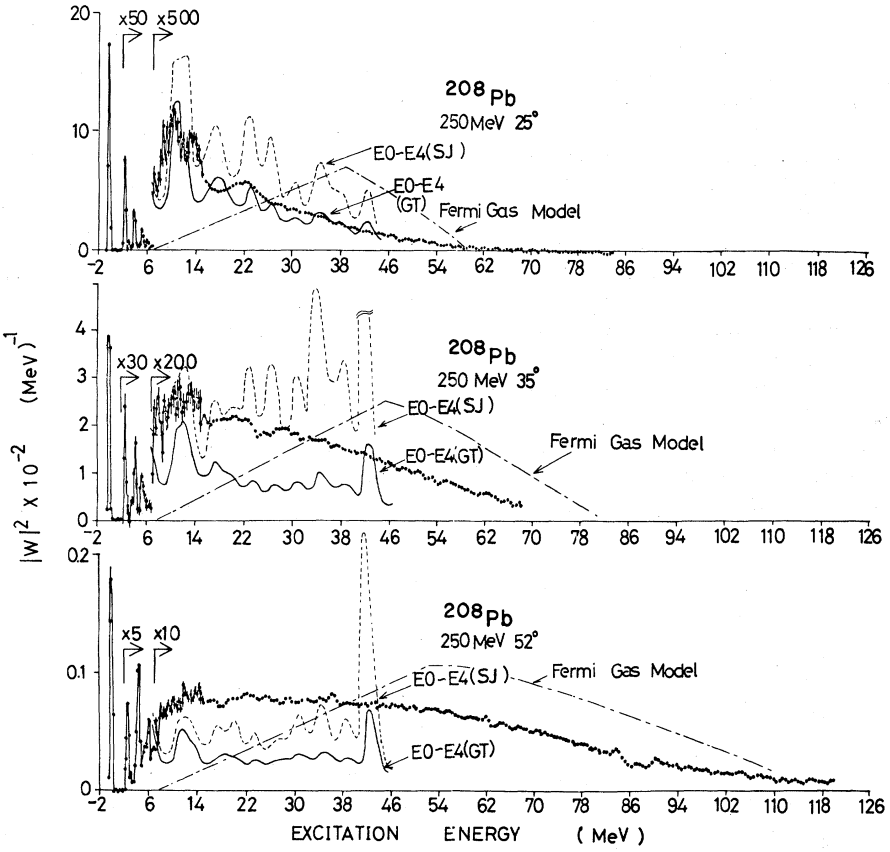

FIG. 4. Spectra in an excitation energy range of ~100 MeV. Dot-dashed curves are those predicted from the Fermi-gas model with $k_f = 265$ MeV, $M^* = 0.8M$, and $\epsilon_B = 7.4$ MeV. The cross sections from $E0$ to $E4$ strength distributions of RPA were calculated using the q dependence of the Tassie model for isoscalar modes and the GT model (full line) or the SJ model (dashed line) for isovector modes are shown.

The observed spectra contain contributions from longitudinal and transverse form factors. We attempted to separate these terms using (3) in PWBA. This formula, however, is not correct for heavy nuclei such as ^{208}Pb and may introduce errors due to the distortion of the electron wave. Nonetheless, we have extracted the transverse part as a function of ω using (3), with the spectra at 250 MeV, 52°, and at 124 MeV, 116° (case 1), with 250 MeV, 52°, and 106.4 MeV, 155° (case 2), and with the three of them by least-square fit (case 3). In these three cases the transverse form factors integrated from 15 to 21 MeV and from 21 to 28 MeV agree well within the statistical error. The result is shown in Fig. 5, where the transverse part is indicated by hatching. The transverse parts in the other spectra were estimated from the result shown in Fig. 5 by assuming the q dependence contained in the Fermi-gas quasielastic model. The transverse contributions to the various spectra are shown by the shaded regions in Fig. 6.

Recently, Lindgren *et al.*[41] observed giant $M2$ states at 7.4 and 7.9 MeV by 180° electron scattering. We have added the contribution from these states to the transverse part mentioned above. The effect of these $M2$ states is negligible in the spectra at forward angles.

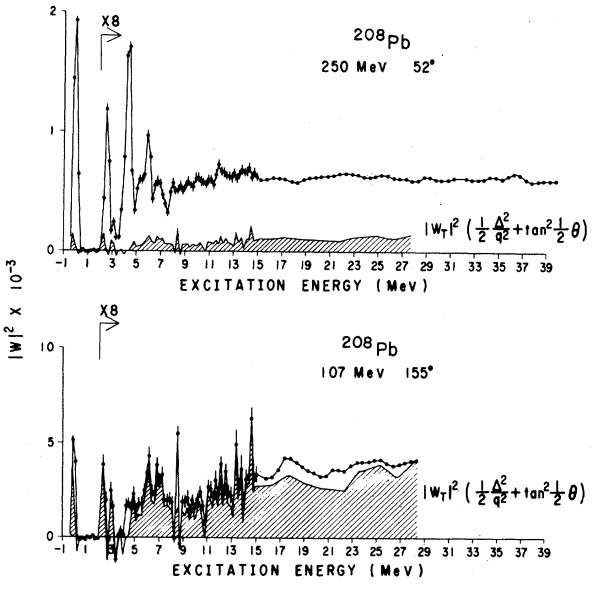

FIG. 5. Spectra at 250 MeV, 50° and 107 MeV, 155° corresponding to the same q_{eff} at an excitation energy of 20 MeV. The separated transverse parts are shown by hatching.

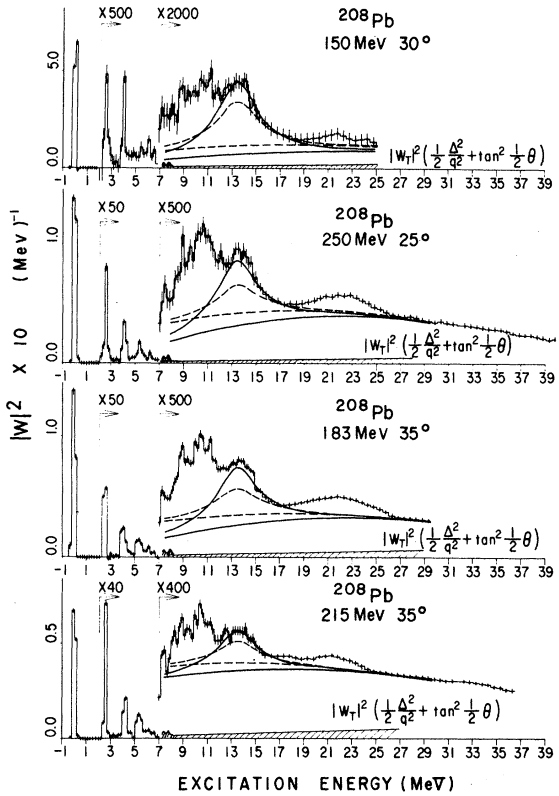

FIG. 6. Spectra of the giant multipole resonance region. Backgrounds were estimated phenomenologically by taking into account the giant dipole resonance calculated with the Goldhaber-Teller (dashed line) and Steinwedel-Jensen (solid line) models. The hatched area is the transverse contribution.

VI. GIANT MULTIPOLE RESONANCES (PHENOMENOLOGICAL ANALYSIS)

The observed spectra at low q and at low excitation energies, as mentioned before, show a large deviation from the quasielastic model. The excess cross section, compared with the single-particle model, implies the excitation of the resonance states in this region. However, since the same processes are involved in the resonance excitation as for quasielastic scattering, these two effects cannot be measured separately. Nonetheless, giant resonances may be identified from (1) their narrow width, (2) definite multipole order, (3) transition strength compared with the sum rule, and (4) systematics of the excitation energy.

Figure 6 shows the ^{208}Pb spectra in the momentum transfer range from 0.447 to 0.714 fm^{-1}. In order to improve the statistical accuracy, three-point smoothing was applied to the region above 15 MeV. Besides the giant dipole resonance (GDR) at 13.5 MeV, dominant peaks are seen centered at 10 and 22 MeV. In the previous analysis[3] the

background was approximated by the form $y=a(\omega-E_0)^{1/n}$, where E_0 was assumed to be 7.4 MeV; n and a are adjustable parameters determined by the fitting procedure. However, this form cannot be applied to the present spectra. Instead we used a power series form given by $y=a_0\sqrt{\omega}+a_1\omega+a_2\omega^2$. The inelastic electron scattering cross section of the GDR for ^{208}Pb is given by $\sigma(\omega)=C\Gamma[(E-\omega)^2+\frac{1}{4}\Gamma^2]^{-1}$, where $\Gamma=4.05$ MeV and C was obtained by multiplying the $B(E1)$ value derived from the (γ,n) cross section[42] by the DWBA cross section normalized to unit value for the $B(E1)$. In the DWBA calculation both GT and SJ models were employed. The GDR cross section and background were simultaneously fitted to the spectra as shown in Fig. 6, where the dashed and solid curves correspond to fitting the GDR with the GT and SJ models, respectively.

The relative cross sections for the resonance part, after subtraction of the GDR and background, in the range 7.4–9.5, 9.5–12, and 18–26 MeV, are plotted in Fig. 7, where open and closed circles correspond to fitting the GDR with the GT and SJ model $E1$ form factors, respectively. For the form factor in the 7.4–9.5 MeV region if the GT model is used to subtract the GDR, the remaining cross section is best reproduced by the GT model $L=1$ form factor. However, if the SJ model is used to subtract the GDR, the remainder can be fitted reasonably well by either a GT model $L=2$ form factor or an SJ model $L=1$ form factor. Thus, this phenomenological analysis does not uniquely determine the dominant multipolarity in the 7.4 to 9.5 MeV excitation region. The 9.5–12 MeV form factor is well reproduced with the theoretical $E2$ form factor given by either the Tassie model or GT model. The form factor between 18 and 26 MeV is in agreement with the $E2$, $T=1$ form factor given by the GT model. The background part integrated from 20 to 25 MeV is also plotted in Fig. 7 and is compared with the cross section calculated from the Fermi-gas model, and with the $E4$ form factor obtained with the GT model. The later curves suggest that the background involves mainly high multipole components. The $B(EL)$ values for the 9.5–12 and 18–26 MeV intervals were found to be 4.6×10^3 and 2.9×10^3 fm^4, respectively.

VII. MULTIPOLE EXPANSION OF THE NUCLEAR CONTINUUM

The ^{208}Pb spectra at 150 MeV, 30°, 250 MeV, 25°, 183 MeV, 35°, 215 MeV, 35°, and 250 MeV,

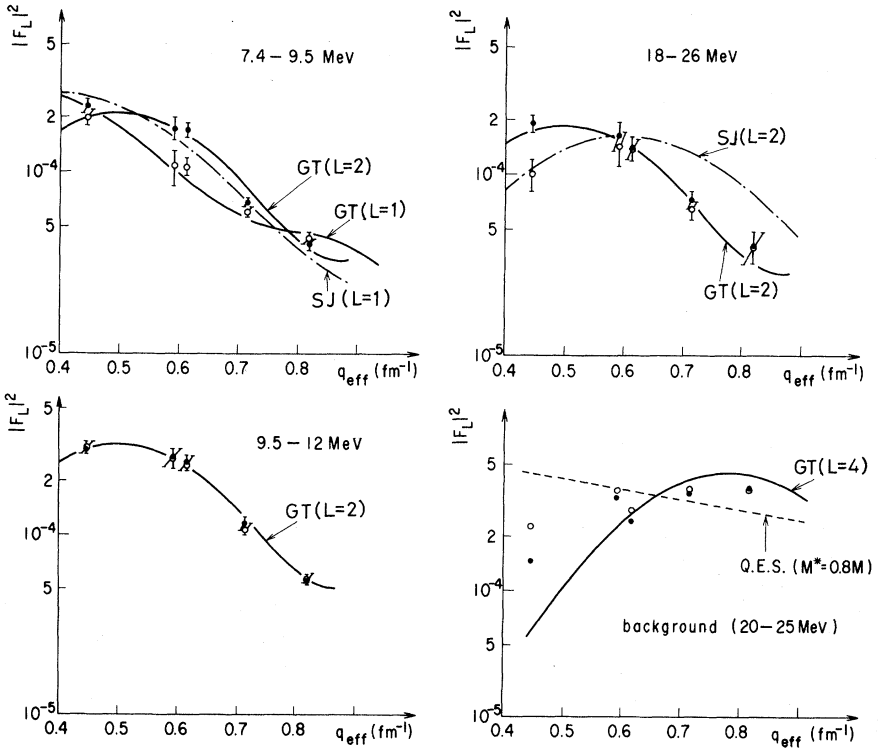

FIG. 7. The cross sections in specific energy ranges for the giant multipole resonances estimated phenomenologically as shown in Fig. 6 are compared with various models. The cross section of the background (right side lower part) is compared with the Fermi-gas model and $L=4$ GT form factor.

35° were decomposed into $E1$, $E2$, $E3$, and higher multipoles by least squares fitting, using the q dependences of the Tassie model for the assumed isoscalar states and the GT or SJ model for the assumed isovector states. The spectra were divided into successive bins of equal intervals of 210 keV in the range below 15 MeV and 500 keV beyond 15 MeV. The contribution of the transverse form factor (the hatched area in Fig. 6) was subtracted. The form factor for each bin corresponding to the same excitation energy is assumed to be the sum of the $E1$, $E2$, $E3$, and higher multipole components:

$$W_c^{(n)} = a_1^n |F_{E1}|^2 + a_2^n |F_{E2}|^2 + a_3^n |F_{E3}|^2 + a_4^n |F_\alpha|^2 ,$$

where $a_i^n \geq 0$, and a_i^n are determined by least-square fitting. The higher multipole term was assumed to be $E4$ (Set I) or the sum of $E4$ and $E5$ (Set II) or the sum of $E4$, $E5$, and $E6$ (Set III), where relative amplitudes among $E4$, $E5$, and $E6$ form factors were determined by normalizing to the corresponding energy-weighted sum rule (EWSR). The $E1$ and $E2$ components of Set III are in good agreement with those of Set II, but do not agree with Set I. We believe that the assumption in Set I may not be realistic. The $E2$ excitation above the GDR is presumably isovector and the other multipoles except for $E1$ were assumed to be isoscalar. The result of the multipole expansion for the spectrum at 183 MeV and 35° is displayed in Fig. 8. The upper portion corresponds to the expansion using the q dependence of the Tassie model for isoscalar and the SJ model for isovector states. The lower portion corresponds to the expansion using the Tassie model for isoscalar and GT model for isovector states. The right-hand scale in Fig. 8 indicates $B(EL)$/MeV, which cannot be applied to the $E2$ strength of the SJ expansion above 17 MeV. The fitting errors shown in Fig. 8 were determined by the contour enclosing $\chi^2 \leq 2\chi^2_{\min}$. The $B(EL)$ values and percentages of the corresponding EWSR for the specific excitation energies are tabulated in Table II. The 6% uncertainty of the DWBA calculation and difference between Set II and Set III were added to the fitting error.

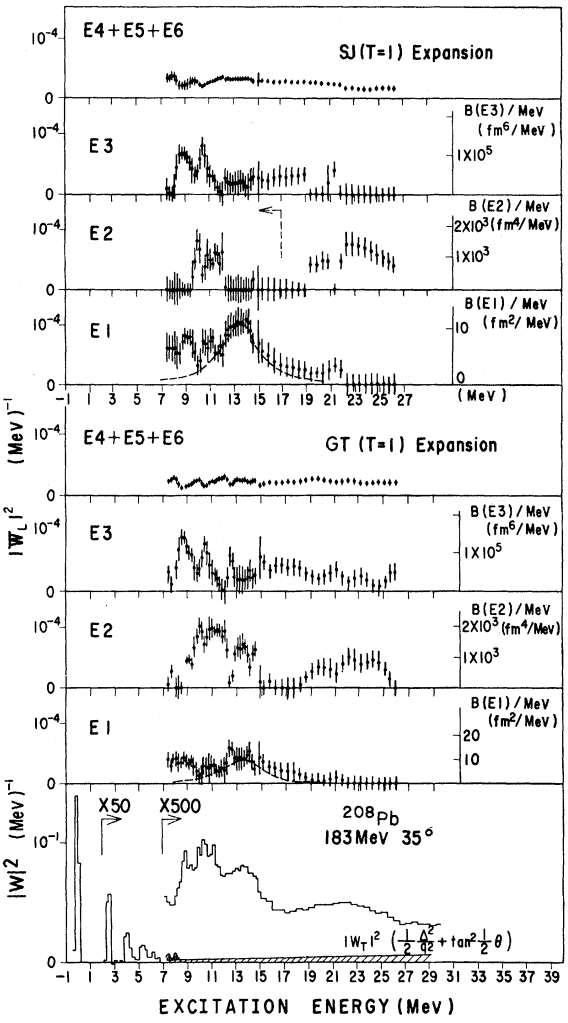

FIG. 8. The spectrum at 183 MeV, 35° was decomposed into spectra for $E1$, $E2$, $E3$, and the sum of $E4$, $E5$, and $E6$ using the q dependence of the Tassie model for the isoscalar mode and the GT model for isovector (lower part) and the SJ model for isovector (upper part). $B(EL)$/MeV at the right-hand side cannot be applied for the $E2$ component of the SJ-model expansion above 17 MeV. Errors are those from fitting. The lowest portion of the figure is the experimental spectrum after radiative unfolding.

The results obtained are discussed as follows.

a. *Giant dipole resonance.* The $E1$ strengths between 9.5 and 26 MeV extracted with the GT and SJ models exhaust, respectively, $(136 \pm {}^{21}_{33})\%$ and $(128 \pm {}^{17}_{29})\%$ of the $E1$ EWSR consistent with $(117 \pm 8)\%$ obtained from the (γ, n) experiment.[42] The GT and SJ form factors corresponding to a 100% EWSR with a Breit-Wigner line profile normalized to a width of 4.05 MeV consistent with the above (γ, n) reaction are shown with the dashed curves in Fig. 8. Both GT and SJ curves reproduce very nicely the experimental $E1$ form factors, while an excess (about 20% of the $E1$ EWSR) is seen in the region from 7.4 to 9.5 MeV. This cross section will be discussed later.

b. *Giant quadrupole resonance.* The peak centered at 22 MeV seen in the primary spectra shifts to 22.5 MeV by this multipole expansion. The $E2$ form factors are concentrated in the same regions centered at 11 and 22.5 MeV in both the GT and SJ model expansions. The deduced $E2$ strengths,

TABLE II. $B(EL)$ values in fm^{2L} and ratios to energy weighted sum rules, obtained by multipole expansion using the Tassie- and GT-model q dependences or the Tassie and SJ q dependences (right).

E_x (MeV)	Expansion with GT model $E1$	$E2$	$E3$ ($\times 10^5$)	Expansion with SJ model for $T=1$ $E1$	$E2$	$E3$ ($\times 10^5$)
7.4–9.5	$19.0^{+2.5}_{-4.0}$	810^{+290}_{-180}	$1.70^{+0.24}_{-0.47}$	$15.0^{+2.1}_{-2.2}$	<160	$1.17^{+0.23}_{-0.49}$
	22% ($T=1$)	9% ($T=0$)	16% ($T=0$)	17% ($T=1$)		11% ($T=0$)
9.5–12	$14.2^{+4.4}_{-6.0}$	4410^{+660}_{-470}	$1.26^{+0.14}_{-0.49}$	$15.2^{+2.7}_{-3.8}$	2620^{+830}_{-480}	$1.25^{+0.23}_{-0.63}$
	21% ($T=1$)	59% ($T=0$)	15% ($T=0$)	22% ($T=1$)	35% ($T=0$)	15% ($T=0$)
12–15	$29.3^{+4.7}_{-5.9}$	3140^{+870}_{-440}	$1.10^{+0.26}_{-0.76}$	$28.5^{+3.2}_{-3.2}$	360^{+660}_{-330}	$0.70^{+0.25}_{-0.70}$
	54% ($T=1$)	53% ($T=0$)	16% ($T=0$)	52% ($T=1$)	6% ($T=0$)	10% ($T=0$)
15–18	$18.3^{+4.5}_{-4.7}$	130^{+580}_{-130}	$1.89^{+0.34}_{-0.46}$	$12.3^{+3.0}_{-3.0}$	<350	$1.1^{+0.33}_{-0.67}$
	41% ($T=1$)	2% ($T=1$)	34% ($T=0$)	28% ($T=1$)		20% ($T=0$)
18–26	$6.6^{+5.0}_{-6.6}$	5260^{+2000}_{-850}	$2.59^{+0.42}_{-1.88}$	$8.8^{+3.0}_{-8.8}$	2310^{+560}_{-330}	$0.74^{+0.45}_{-0.74}$
	20% ($T=1$)	94% ($T=1$)	63% ($T=0$)	26% ($T=1$)	41% ($T=1$)	18% ($T=0$)

however, depend upon the model employed, i.e., the sum of the $E2$ strengths in the region 7.4–15 MeV exhausts $(120 \pm {}^{25}_{12})\%$ and $(42 \pm {}^{15}_{8})\%$ of the isoscalar $E2$ EWSR for the expansion with the GT and SJ models, respectively. The $E2$ form factor in the region around 23 MeV may be attributed to $T=1$ and exhausts $(95 \pm {}^{40}_{13})\%$ and $(41 \pm {}^{12}_{6})\%$ of the isovector $E2$ EWSR for the GT and SJ expansion, respectively.

c. Giant octupole resonance. The $E3$ excitations appear as narrow peaks at ~8.5 and ~10.3 MeV and a broad bump centered at ~16 MeV. The former two may correspond to the $1\hbar\omega$ shell model transition and the latter may correspond to the $3\hbar\omega$ transition. Since the isoscalar collective 3^- state is observed at 2.61 MeV the $E3$ component around 9 MeV may be considered to be isovector. Nonetheless, the sum of the $E3$ strengths in the range 7.4–26 MeV was compared with the isoscalar sum rule and obtained $(165 \pm {}^{15}_{71})\%$ and $(94 \pm {}^{14}_{47})\%$ of the $E3$ EWSR with GT and SJ expansions, respectively. It may be interesting to note that the fine structure observed around 9 MeV in the primary spectra is not due to a single multipole, but may be a complex of $E1$, $E2$, and $E3$.

VIII. DISCUSSION AND CONCLUSION

In this section we give some detailed discussion on the individual character of the giant multipole resonances.

A. Giant dipole resonance

The most serious problem in the present multipole expansion is the nuclear model employed, because the difference between the GT- and SJ-model form factors is rather large.[43] The Hartree-Fock RPA for the isovector GDR predicts two dipole peaks for all the spherical nuclei calculated, e.g., in ^{208}Pb a peak at 12.2 MeV and another at 16.1 MeV (Ref. 39). The lower state has ρ_{tr} resembling the SJ model, while the upper state has ρ_{tr} resembling the GT model. The transition density corresponding to the macroscopic model was derived from a reduction of RPA.[44] This calculation gives the GT shape for light nuclei, and a shape between the GT and SJ models for ^{208}Pb. The Tamm-Dancoff calculation[45] of the dipole state in ^{208}Pb with 45 single-particle states predicts the main peak at 13.3 MeV and small peaks at 11.3, 11.1, and 10.7 MeV. The transition density for the main peak resembles the GT model, while the lower peaks resemble the SJ model. However, for the dipole states in ^{40}Ca, ^{90}Zr, and ^{116}Sn only the GT shape was predicted.

In Fig. 8 an excess $E1$ cross section, compared with the resonance line shape obtained from the (γ, n) reaction,[42] is seen in the region of the particle emission threshold energy. The total photon-absorption cross section for lead in the threshold region is smaller than the present $E1$ strength in this region.[46] If, however, we assume, as suggested by the shell model,[45] the GT model state for the upper part of the GDR and the SJ model state for the lower part, this discrepancy may partly be solved. Spurious states may arise from instrumental scattering, unfolding of the radiation tail, and the procedure of multipole expansion.

The background from the instrument seems to be broad and appears, due to the large contribution of the elastic peak, mostly in spectra at low momentum transfers. Hence, such contribution may be seen on the shape of the decomposed GDR. However, we have obtained the well-known GDR shape at excitation energies above 10 MeV. The error of the unfolding may spread over the whole area and not concentrate in a small region. The same multipole expansion procedure was applied to the ^{90}Zr spectra.[36] However, only small $E1$ strength was observed below 10 MeV in contrast to the ^{208}Pb case. We need more investigations for the cross section near the threshold energy.

B. Giant monopole resonance

Although many microscopic and macroscopic theories[38-40,47-64] have predicted the existence of a giant monopole resonance, there is little conclusive experimental evidence for a collective 0^+ state. A difficulty arises because electron scattering cannot distinguish between $E0$ and $E2$ excitations.

In Table II, if we assume the GT model, the sum of the $E2$ strengths in the region 7.5–15 MeV exhausts $(120 \pm {}^{25}_{12})\%$ of the isoscalar $E2$ EWSR. The $E2$ strength (16%) of the bound state [4.07 MeV 2^+ state, $B(E2)_{exp} = 2920$ $(e^2\,\mathrm{fm}^4)$][65,66] should be added to this sum. The excess $E2$ strength, compared with the sum rule, may imply the existence of an $E0$ resonance in this region.

Evidence for an $E0$ resonance (50% of EWSR) in ^{208}Pb at 8.9 MeV has been presented by Pitthan *et al.*[67] The main reason for the $E0$ assignment given is that this level is excited by electron scattering, but not seen in the (γ, n) reaction. According to the present multipole expansion, however, the cross section near 8.9 MeV is not a single multipole but may be a complex of $E1$, $E2$, and $E3$.

Other evidence for an $E0$ resonance in ^{208}Pb has been presented from 80-MeV deuteron inelastic scattering by Marty *et al.*[12] They have obtained a cross section at 13.5 MeV in the measurement at angles where an $E0$ excitation is favored.

The $E2$ cross section obtained by the GT expansion shows peaks at 10.5 and 13.5 MeV. Inelastic hadron scattering ^{208}Pb spectra indicate the presence of the corresponding $E2$ peak at 10.5 MeV with a rather narrow width of ~3 MeV, but no structure other than a small tail is seen at 13.5 MeV. If one assumes the presence of an $E0$ excitation at 13.5 MeV instead of $E2$, this discrepancy may be removed because electrons can excite strongly both $E0$ and $E2$, whereas hadrons excite $E2$ strongly but $E0$ only weakly except for specific angles. The $E0$ strength between 12.5 and 15 MeV is found to be $(97 \pm {}^{27}_{14})\%$ of the isoscalar $E0$ EWSR and the remaining $E2$ strength between 7.4 and 12.5 MeV exhausts about $(76 \pm {}^{14}_{8})\%$ of the isoscalar EWSR. However, the strength at 13.5 MeV vanishes if we use the SJ model for the GDR.

TABLE III. Percentages of the EWSR in ^{208}Pb below 26 MeV. Contributions from bound states (16% for $T=0$ $E2$ and 20% for $T=0$ $E3$) are included.

Multipole	Mode	ω (MeV)	GT expansion (%)	SJ expansion (%)
$E0$	$T=0$	12.5–15	97^{+27}_{-14}	10^{+20}_{-9}
$E1$	$T=1$	7.4–26	156^{+23}_{-35}	145^{+18}_{-30}
$E2$	$T=0$	7.4–12.5	92^{+14}_{-8}	52^{+12}_{-5}
$E2$	$T=1$	15–26	95^{+40}_{-13}	41^{+12}_{-8}
$E3$	$T=0$	7.4–26	165^{+15}_{-71}	94^{+14}_{-47}

The cross section near 13.5 MeV may be seen in the primary spectra in Fig. 6. Compared with the smooth curves of the Breit-Wigner resonance shape, the measured cross section indicates a structure beyond the experimental error. If we subtract the GDR part, the residual cross section around 13.5 MeV is consistent with the result of the multipole expansion. The sum-rule values for ^{208}Pb in the range below 26 MeV including those of the bound states (16% for $T=0$ $E2$ and 20% for $T=0$ $E3$)[65,66,69] are tabulated in Table III.

The monopole energies predicted by theories depend on the assumed interaction. The observed $E0$ excitation at 13.5 MeV is in agreement with the RPA prediction by Speth, Zamick, and Ring *et al.*[54] and consistent with sum-rule approaches.[61,62] Using the nuclear compressibility consistent with the nuclear saturation property the monopole excitation energy in ^{208}Pb is suggested by Zamick[63] in the range from 12.6 to 16.8 MeV.

C. Giant quadrupole resonance

Many theories[38-40,47,56,70-72] predict $E2$ ($T=0$ and $T=1$) giant resonances for ^{208}Pb below 26 MeV. For example, Suzuki[47] has predicted $E2$ ($T=0$) and $E2$ ($T=1$) at 9.7 and 22 MeV, respectively. The $E2$ strengths in Table III are compared with the finite Fermi-system calculation with 95 single-particle transitions by Kamerdzhiev.[70] In this calculation the theoretical lowest 2^+ state is found at 4.15 MeV and has a strength of $\mathrm{EWSR}_{th} = 17.9\%$ ($T=0$), which is in good agreement with the experimental value[65,66]; $\omega_{exp} = 4.07$ MeV and $\mathrm{EWSR}_{exp} = 16\%$. The theoretical 2^+ states at 9.51, 10.05, 11.01, and 11.84 MeV have a strength of EWSR_{th}

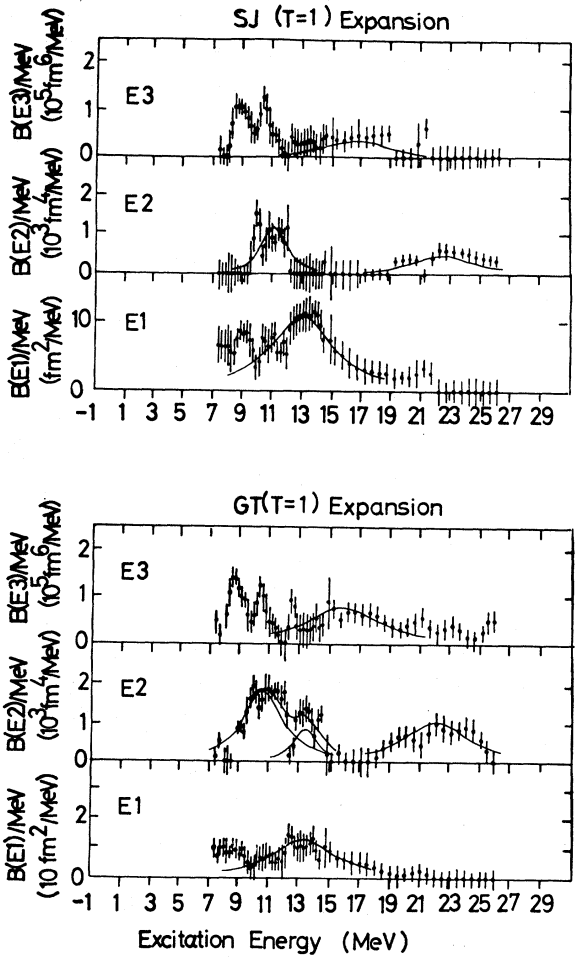

FIG. 9. The Breit-Wigner line shape fit to the $E1$, $E2(E0)$, and $E3$ strength distributions obtained by multipole expansion.

$= 82\%$ ($T = 0$), which is in agreement with the values of the GT expansion; $\omega_{exp} \simeq 10.8$ MeV and $T = 0$ $EWSR_{exp} = (76 \pm {}^{14}_{8})\%$ in the range 7.4–12.5 MeV. Theory predicts the $T = 1$ $E2$ giant resonance states between 18.85 and 22.71 MeV with a strength of $T = 1$ $EWSR_{th} = 113\%$ in agreement with the values of the GT expansion; $\omega_{exp} \simeq 22.5$ MeV and $T = 1$ $EWSR_{exp} = (95^{+40}_{-13})\%$.

In Fig. 9, $E1$, $E2(E0)$, and $E3$ strength distributions are fitted with a Breit-Wigner line shape by the least-squares method. The excitation energies, line widths, and transition strengths determined are tabulated in Table IV. Rather consistent results between the different models for positions, widths, and strengths indicate that the present multipole expansion is satisfactory. It is noticed that the transition strengths obtained from this fitting are much larger than those in Table III, because the Breit-Wigner line shape includes the contribution from the tail.

TABLE IV. Strengths, center energies, and widths obtained by the Breit-Wigner line shape fit to multipole components in Fig. 9.

ω (MeV)	Mode	Γ (MeV)	$B(EL)$ or $\lvert\langle r^2\rangle\rvert^2$
	GT expansion		
13.6	$E1(T=1)$	5.0	90 fm^2
10.8	$E2(T=0)$	3.2	9000 fm^4
13.6	$E2(T=0)$	1.8	2400 fm^4
	or $E0(T=0)$	1.8	4700 fm^4
22.5	$E2(T=1)$	5.0	8100 fm^4
16.0	$E3(T=0)$	6.0	5.2×10^5 fm^6
	SJ expansion		
13.1	$E1(T=1)$	5.0	80 fm^2
11.0	$E2(T=0)$	2.0	3800 fm^4
22.5	$E2(T=1)$	5.0	2700 fm^4
16.6	$E3(T=0)$	5.4	2.3×10^5 fm^6

Isospin-zero projectiles can excite only isoscalar states. Inelastic α-particle scattering[68] from ^{208}Pb has found a $T = 0$, 2^+ state at 11 MeV with a width of ~3 MeV which is in good agreement with the values of the GT expansion; $\omega = 10.8$ MeV and $\Gamma = 3.2$ MeV.

D. Giant octupole resonance

The giant octupole resonance states are made up from the $1\hbar\omega$ and $3\hbar\omega$ shell model transitions. Accordingly, the separation of the isoscalar and isovector states is very complicated. The octupole strength is composed of peaks at 8.5 and 10.3 MeV and a broad bump centered at ~16 MeV. In Fig. 9 the bump is fitted with a Breit-Wigner resonance shape. The values obtained are: $\omega = 16$ MeV, $\Gamma = 6$ MeV, and $B(E3) = 5.3\times10^5$ (fm^6) (GT expansion) and $\omega = 16.6$ MeV, $\Gamma = 5.4$ MeV, and $B(E3) = 2.3\times10^5$ (fm^6) (SJ expansion).

E. Higher multipole resonances

Strengths for the higher multipole resonances seem to underlie the entire spectrum with a quite flat energy dependence. This strength approaches that of the background used in the phenomenological analysis.

The excitation energies and transition strengths of the giant multipole resonances in ^{208}Pb obtained by different measurements are summarized in Table V. We find approximately the same positions for the giant multipole resonances except for monopole. For the transition strengths, however, large discrepancies between the different measurements are seen.

TABLE V. Excitation energies and percentages of the corresponding EWSR in ^{208}Pb. The errors of the present data include statistical and fitting uncertainties (Table II) and also differences between models (see the text).

		2^+ $(T=0)$		0^+ $(T=0)$		1^- $(T=1)$		2^+ $(T=1)$		3^- $(T=0)$	
Experiment	Ref. No.	ω (MeV)	EWSR (%)	ω (MeV)	EWSR (%)	ω (MeV)	EWSR (%)	ω (MeV)	EWSR (%)	ω (MeV)	EWSR (%)
(e,e')	3	8.9 9.4 10.0 10.6	~47					22	~60	19	~44
(e,e')	73	10.2 10.6 11.2	~35			14.1					
(e,e')	67	10.5	95	8.9	50	13.6	105,205	22.5	85	17.5	90
(e,e')	74	8.9 10.8	35 80			14.1					
(p,γ)	75							23.7			
(γ,n)	76	9.034 9.421 10.06	15 25 48								
(p,p')	5	11.2									
(α,α')	68	10.8									
(d,d')	12	10.8	32±5	13.5	60–100						
(e,e')	This work[a]	11	30–82	13.6	1–124	13.6	115–179	22.5	33–135	16	47–180

[a] Excitation energies obtained by the GT expansion.

From the experimental[10] and theoretical[11] studies of the collective states, we may say that the Tassie or GT model may correspond to the upper limit of the transition density located far outside of the nucleus. On the other hand, the SJ model may correspond to the lower limit of the transition density located inside of the nucleus. We then regard the GT and SJ models as giving the upper and lower limits of the $B(EL)$, respectively. The EWSR values thus evaluated are shown in Table V.

We again compare the present result with the RPA. The excitation energies and strengths predicted from the RPA[38-40] for the low-lying collective states are compared with the experimental values[66,69] in Table VI. The RPA is in good agreement with experiment, i.e., the predicted strengths[40] are within 10% of the experimental val-

TABLE VI. The RPA calculations for the low-lying collective states in ^{208}Pb are compared with the experimental data of Refs. 62 and 65. $B(EL)$ is in Weisskopf units.

	Experiment		RPA values: Ring and Speth[a]		Bertsch and Tsai[b]		Liu and Brown[c]	
J^π	ω (MeV)	(W.u.) $B(EL)$	ω (MeV)	$B(EL)$ (W.u.)	ω (MeV)	$B(EL)$ (W.u.)	ω (MeV)	$B(EL)$ (W.u.)
3^-	2.61	36±3	2.64	31	2.7	29	2.8	38
5^-	3.19	11.1±1.4	3.39	7	3.3	6	3.4	14
5^-	3.71	8±2	3.82	8				
2^+	4.07	8.1	4.49	8.5	5.4	7	5.6	7
4^+	4.32	15	4.69	9	5.4	7	6.4	16
6^+	4.42	11.7	4.77	11				

[a] From Ref. 38.
[b] Reference 39.
[c] Reference 40.

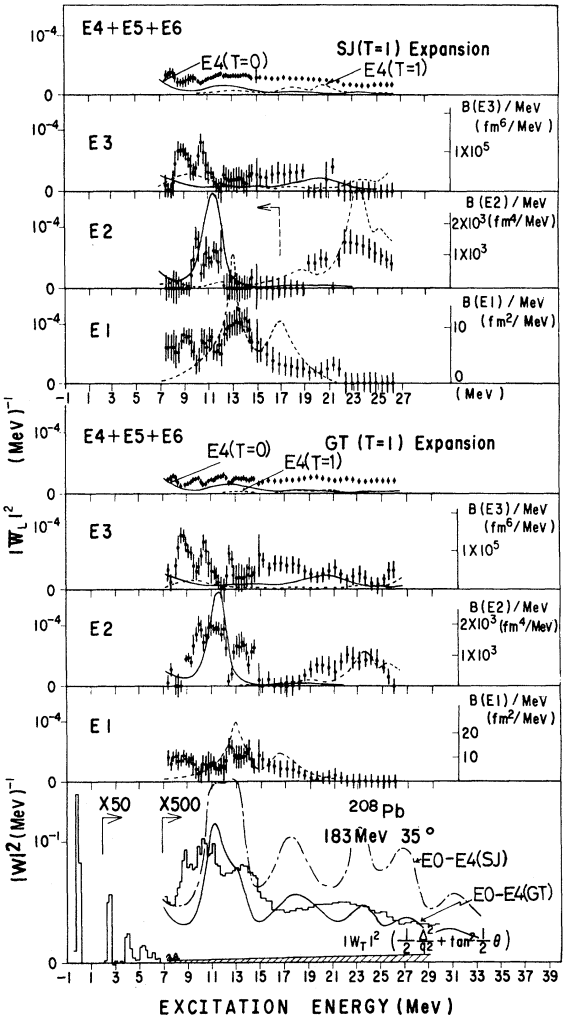

FIG. 10. Comparison of the multipole strength distributions between the RPA theory and the present analysis. The cross section from the RPA strength distributions were calculated by the q dependence of the Tassie model for isoscalar and the GT model for isovector (lower part) and the SJ model (upper part). The solid and dashed curves are the calculation for the $T=0$ and $T=1$ states, respectively. In the lowest portion the sum of $E0$ to $E4$ cross sections of the RPA are shown by the full line (using the Tassie- and GT-model q dependences) and the dot-dashed line (using the Tassie- and SJ-model q dependences). The $B(EL)$/MeV scale cannot be applied for the $E2$ component of the SJ expansion above 17 MeV.

ues. The RPA strengths for the $E0$ ($T=0$), $E1$ ($T=1$), $E2$ ($T=0$), $E2$ ($T=1$), and $E3$ ($T=0$) giant resonances integrating up to 25 MeV exhaust 88, 92, 72, and 80%, respectively, of the corresponding EWSR[40] which involve the effect of the exchange term. The form factors from the $E0$, $E1$, $E2$, $E3$, and $E4$ strengths of the RPA were calculated using the q dependence of the Tassie model for isoscalar and the GT or SJ model for isovector states. The results are shown in Fig. 10 where the solid and dashed curves are the calculation for the $T=0$ and $T=1$ states, respectively. The experimental form factors are in good agreement with those obtained by the GT model but do not agree with those by the SJ model.

It should be noticed that the $E3$ strength around 8.5 MeV is much larger than that of the RPA. The possibility for the excitation of the isoscalar GDR around these energies is suggested by Speth *et al.*[77]

We may conclude the following: (a) Unfolding of the radiation tail has been improved. (b) A large background still lies under the giant resonance peaks, nonetheless. (c) Comparison between theory and experiment suggests that the observed spectra at small values of q and ω may be a sum of the multipole resonance states. (d) A multipole expansion procedure which can predict the position and strength of any multipole resonance states was applied to the observed spectra. (e) In this new analysis, the well-known giant dipole resonance is clearly seen. (f) The $E2$ resonance both above and below the energy of the dipole resonance are consistent with those of the phenomenological analysis. (g) The isoscalar and isovector $E2$ strengths obtained by the combination of the Tassie ($T=0$) and GT ($T=1$) models exhaust a significant fraction of the corresponding EWSR, while their strengths decrease to values less than half of the EWSR when the SJ model for $T=1$ states is employed. (h) A monopole resonance which exhausts the sum rule is suggested at 13.5 MeV if the GDR is subtracted with the GT model, but this vanishes if the SJ model is employed. (i) The RPA strengths for $E0$ ($T=0$) and $E2$ ($T=0$ and $T=1$) are in good agreement with the experimental values obtained by the q dependence of the GT model for $T=1$ states, but do not agree with those obtained by the SJ model. (j) There may be a giant octupole resonance at ~16 MeV. (k) A complicated structure around 9 MeV seems to be a complex of different multipole states. (l) The nuclear continuum underlying the resonances is largely explained as being due to overlapping of many multipole resonance states.

ACKNOWLEDGMENT

We are grateful to Dr. J. Friedrich for his valuable contributions on the unfolding of the radiative effects during his stay at our laboratory. We are also indebted to Professor Y. S. Tsai on the subtraction of the radiation tail. We are thankful to Dr. Y. Kawazoe for the use of his

DWBA code for the monopole excitation, and to Professor G. A. Peterson and Professor T. W. Donnelly for their valuable comments. We also thank our friends at our laboratory for their help in the data taking and for the operation of the machine during the course of the present experiment. The computer center at Tohoku University was used for the DWBA calculation.

---

*Maiden name: Mamiko Nagao.
[1]R. Pitthan and T. Walcher, Phys. Lett. 36B, 563 (1971).
[2]S. Fukuda and Y. Torizuka, Phys. Rev. Lett. 29, 1109 (1972).
[3]M. Nagao and Y. Torizuka, Phys. Rev. Lett. 30, 1068 (1973).
[4]M. B. Lewis and F. E. Bertrand, Nucl. Phys. A196, 337 (1972).
[5]G. R. Satcheler, Phys. Rep. 14C, 98 (1974).
[6]Y. Torizuka, K. Itoh, Y. M. Shin, K. Kawazoe, H. Matsuzaki, and G. Takeda, Phys. Rev. C 11, 1174 (1975).
[7]K. Hosoyama and Y. Torizuka, Phys. Rev. Lett. 35, 199 (1975).
[8]J. Friedrich, Nucl. Instrum. Methods 129, 505 (1975).
[9]M. B. Lewis, Phys. Rev. C 9, 1878 (1974).
[10]K. Itoh, M. Oyamada, and Y. Torizuka, Phys. Rev. C 2, 2181 (1970).
[11]G. Bertsch and S. F. Tsai, Phys. Lett. 50B, 319 (1974).
[12]N. Marty, M. Morlet, A. Willis, V. Comparat, R. Frascaria, and J. Kalline (unpublished).
[13]T. de Forest and J. D. Walecka, Adv. Phys. 15, 1 (1966).
[14]A. Yamaguchi, T. Terasawa, K. Nakahara, and Y. Torizuka, Phys. Rev. C 3, 1750 (1971).
[15]D. G. Ravanhall, quoted in R. Hofstadter, Rev. Mod. Phys. 28, 214 (1956).
[16]S. T. Tuan, K. E. Wright, and D. S. Onley, Nucl. Instrum. Methods 60, 70 (1968).
[17]L. J. Tassie, Aust. J. Phys. 9, 407 (1956).
[18]H. Uberall, *Electron Scattering from Complex Nuclei* (Academic, New York, 1971), Part B, Chap. 6.
[19]J. V. Noble, Ann. Phys. (N.Y.) 67, 98 (1971).
[20]T. J. Deal and S. Fallieros, Phys. Rev. C 7, 1709 (1974).
[21]H. Ui and T. Tsukamoto, Progr. Theor. Phys. 51, 1377 (1974).
[22]M. Goldhaber and E. Teller, Phys. Rev. 74, 1046 (1948).
[23]H. Steinwedel, J. H. D. Jensen, and P. Jensen, Phys. Rev. 79, 1109 (1950).
[24]H. Euteneuer, J. Friedrich, and N. Voegler, Phys. Rev. Lett. 36, 129 (1976).
[25]J. Heisenberg *et al.*, Phys. Rev. Lett. 23, 1402 (1969).
[26]G. R. Satchler, Nucl. Phys. A195, 1 (1972).
[27]M. Kimura *et al.*, Nucl. Instrum. Methods 95, 403 (1971).
[28]M. A. Duguay, C. K. Bockelman, T. H. Curtis, and K. A. Eisenstein, Phys. Rev. 163, 1259 (1967).
[29]H. Uberall, *Electron Scattering from Complex Nuclei* (see Ref. 18), Chap. 6, p. 514. Here the cross section from one-bin $(d\sigma/d\Omega)^{(n)}$ corresponds to that from one level.
[30]L. C. Maximon, Rev. Mod. Phys. 41, 193 (1969).
[31]B. Rossi, *High Energy Particles* (Prentice-Hall, New Jersey, 1956).
[32]U. Chaloupka *et al.*, Phys. Lett. 50B, 1 (1974).
[33]L. W. Mo and Y. M. Tsai, Rev. Mod. Phys. 41, 205 (1969).
[34]L. C. Maximon and D. B. Isabelle, Phys. Rev. 136B, 674 (1964).
[35]Y. S. Tsai, Stanford Linear Accelerator Report No. SLAC-PUB-848, 1971 (unpublished).
[36]S. Fukuda and Y. Torizuka, Phys. Lett. 62B, 146 (1976).
[37]E. J. Moniz, I. Sick, R. R. Whitney, J. R. Ficenec, R. D. Kephart, and W. P. Trower, Phys. Rev. Lett. 26, 445 (1971).
[38]S. Krewald and J. Speth, Phys. Lett. 52B, 295 (1974).
[39]G. Bertsch and S. F. Tsai, Phys. Rep. 18C, 125 (1975).
[40]K. E. Liu and G. E. Brown (unpublished).
[41]R. A. Lindgren, W. L. Bendel, L. W. Fagg, and E. C. Jones, Jr., Phys. Rev. Lett. 35, 1423 (1975).
[42]A. Veyssiere, H. Beil, R. Bergere, P. Carlos, and A. Lepretre, Nucl. Phys. A159, 561 (1970).
[43]M. Buenerd, P. de Saintignon, P. Martin, and J. M. Loiseaux, Phys. Rev. Lett. 33, 1233 (1974).
[44]G. Bertsch and K. Striker, Phys. Rev. C 13, 1312 (1976).
[45]H. Sagawa, in Proceedings of the Kawatabi Conference on New Giant Resonances [Research Report of the Laboratory of Nuclear Science, (1975), Vol. 8, supplement].
[46]E. G. Fuller and E. Hayward, Nucl. Phys. 33, 431 (1962).
[47]T. Suzuki, Nucl. Phys. A217, 182 (1973).
[48]G. R. Hammerstein, H. McManus, A. Moalem, and T. T. S. Kuo, Phys. Lett. 49B, 235 (1974).
[49]V. R. Pandharipande, Phys. Lett. 31B, 635 (1970).
[50]E. Caurier, B. Bourotte-Bilwes, and V. Abgrall, Phys. Lett. 44B, 411 (1973).
[51]S. K. M. Wong, G. Saunier, and B. Rouben, Nucl. Phys. A169, 294 (1971).
[52]J. Damgaard, V. V. Gortchakov, G. M. Vagradov, and A. Molinari, Nucl. Phys. A121, 625 (1968).
[53]D. H. Jakubassa, Z. Phys. 268, 409 (1974).
[54]J. Speth, L. Zamick, and P. B. Ring, Nucl. Phys. A232, 1 (1974).
[55]P. Ring and J. Speth, Phys. Lett. 44B, 477 (1973).
[56]P. Ring and J. Speth, Nucl. Phys. A235, 315 (1974).
[57]H. Flocard and D. Vautherin, Phys. Lett. 55B, 259 (1975).
[58]S. Krewald, J. E. Galonska, and A. Faessler, Phys. Lett. 55B, 267 (1975).
[59]E. C. Halbert, J. B. McGrory, and G. R. Satchler, Nucl. Phys. A245, 189 (1975).
[60]H. Sagawa, Institute for Nuclear Study, University of Tokyo INS Report No. 250 (unpublished).
[61]J. Martorell, O. Bohigas, S. Fallieros, and A. M. Lane, Phys. Lett. 60B, 313 (1976).
[62]E. Lipparini, G. Orlandini, and R. Leonardi, Phys. Rev. Lett. 36, 660 (1976).
[63]L. Zamick, Phys. Lett. 45B, 313 (1973).

[64]E. Grecksch, W. Knüpfer, and M. G. Huber, Lett. Nuovo Cimento 14, 505 (1975).
[65]J. F. Ziegler and G. A. Peterson, Phys. Rev. 165, 1337 (1968).
[66]M. Nagao and Y. Torizuka, Phys. Lett. 37B, 383 (1971).
[67]R. Pitthan, F. R. Buskirk, E. B. Dally, J. N. Dyer, and X. K. Maruyama, Phys. Rev. Lett. 33, 849 (1974).
[68]J. M. Moss, C. M. Roza, J. D. Bronson, and D. H. Youngblood, Phys. Lett. 53B, 51 (1974).
[69]M. Nagao, in *Proceedings of the International Conference on Nuclear Structure Studies Using Electron Scattering and Photoreactions, Sendai, 1972,* edited by K. Shoda and H. Ui (Tohuku Univ., Sendai, Japan, 1972).
[70]S. P. Kamerdzhiev, Phys. Lett. 47B, 147 (1973).
[71]I. Hamamoto, in *Proceedings of the International Conference on Nuclear Structure Studies Using Electron Scattering and Photoreaction, Sendai, 1972* (see Ref. 69).
[72]D. R. Bes, R. A. Broglia, and B. S. Nilsson, Phys. Rep. C 16, 1 (1975).
[73]F. R. Buskirk *et al.*, Phys. Lett. 42B, 194 (1972).
[74]A. Schwierczinski *et al.*, Phys. Rev. Lett. 35, 1244 (1975).
[75]K. A. Snover, K. Ebisawa, D. R. Brown, and P. Paul, Phys. Rev. Lett. 32, 317 (1974).
[76]N. K. Sherman, H. M. Ferdinande, K. H. Lokan, and C. K. Ross, Phys. Rev. Lett. 35, 1215 (1975).
[77]J. Speth *et al.* (private communication).